Lawrence Berkeley National Laboratory
Recent Work

Title
FIGURE CONTROL FOR A FULLY SEGMENTED TELESCOPE MIRROR

Permalink
https://escholarship.org/uc/item/21b281n6

Authors
Mast, T.S.
Nelson, J.E.

Publication Date
1981-12-01

Lawrence Berkeley Laboratory
UNIVERSITY OF CALIFORNIA

Physics, Computer Science & Mathematics Division

FIGURE CONTROL FOR A FULLY SEGMENTED
TELESCOPE MIRROR

Terry S. Mast and Jerry E. Nelson

December 1981

DISCLAIMER

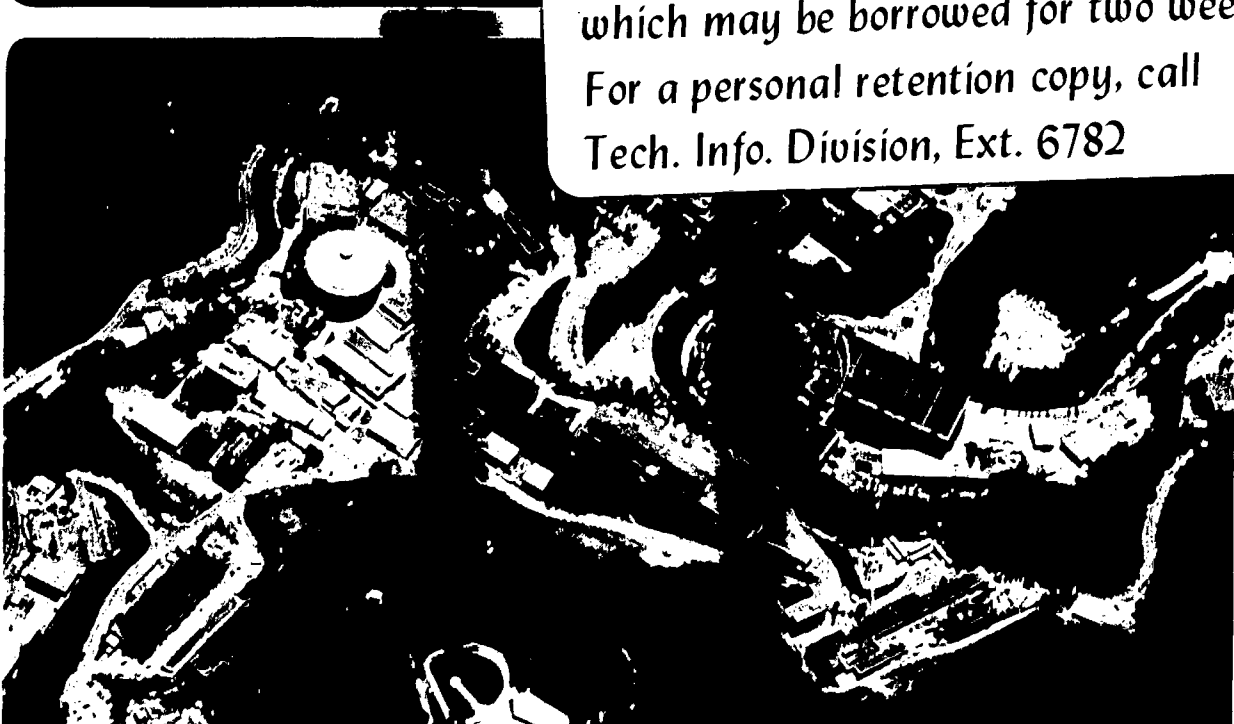# Figure Control For A Fully Segmented Telescope Mirror

Terry S. Mast and Jerry E. Nelson

Lawrence Berkeley Laboratory
University of California
Berkeley, California 94720

December 1981

ABSTRACT

We describe a system to control the figure of a large telescope primary mirror that is composed of many individual segments. The geometry considered, employing hexagonal mirrors, allows a simple and economical control system. The system is shown to be reliable and effective in continuously maintaining the figure to the precision required for optical astronomy.

Figure Control For A Fully Segmented Telescope Mirror

Terry S. Mast and Jerry E. Nelson

Lawrence Berkeley Laboratory
University of California
Berkeley, California 94720

December 1981

Contents

1. Introduction

The cost of large primary mirrors for astronomical telescopes can be greatly reduced by using an assembly of small mirror segments instead of one large solid mirror. The cost of producing small mirrors is less and the risk of catastrophic breakage is virtually eliminated. The weight of the total mirror is also reduced, allowing a simplified and less expensive support structure. In addition fabrication and handling equipment such as aluminizing tanks and cranes are substantially reduced in scale and cost. The mirror segmentation geometry described in this paper, employing hexagonal segments, allows a simple and economical control system. Analysis of this system shows it to be reliable and effective in continuously maintaining the figure to the precision required for optical astronomy.

The central problem with a segmented primary is to assemble the small mirrors and maintain their orientations and positions so that they form the figure of a single large optical quality mirror. We describe here the analysis of a control system designed for a mirror composed of many hexagonal elements. By control system we mean an array of sensors to measure the relative positions and orientations of the mirror segments, an array of actuators to move and correct the segment orientations, and an algorithm for translating the sensor information into the desired actuator motions. The control system is used to monitor the figure of the primary mirror (once it is established) and to continuously preserve it against distortions induced by wind, gravity loading, and temperature changes. We emphasize that this system is a *stabilization* system. The problems and techniques of the initial alignment will be discussed in a future publication.

This analysis is part of a much larger project to design a fully steerable ten meter telescope for the University of California (Nelson, 1977,1979,1980a). The broader goals of the telescope design include: image quality that is limited by atmospheric seeing, not by optical aberrations; a wide angular field (about 20 minutes); capability for observations from 0.3 to 30 microns; and of course economy in construction and operation. Other aspects of the telescope design are described in other publications and a series of technical reports. These include

descriptions of the mirror segment fabrication; the design, production, and testing of mirror position sensors and actuators; alignment procedures; mirror support; telescope optics; telescope structure; and the observatory building and dome.

A control system study similar to the one described here was made for an earlier design of the segment geometry (Mast and Nelson, 1980). That earlier design for this telescope required a large central reference mirror and employed more segments. The new simplified geometry described here requires a slightly more complex set of sensors. The function of the central mirror is provided by a tilt (angle) sensor in the current design. The basic conclusions of the previous study, including the system's imaging characteristics and its ability to be used with even larger arrays of segments, remain valid for the new design.

In the past segmented mirror systems have used a variety of techniques for sensing the segment orientations. Systems using the center of curvature for interferometric sensing of the mirror figure have been used successfully (Crane, 1969). However, to limit the size of the telescope structure, we have avoided requiring access to the center of curvature. Systems employing starlight are also feasible and sensing can be done at the focus (Hardy, 1977). However, the desire to observe in daylight and a rather limited angular field make this technique unattractive for the ten meter telescope. Other techniques employing light beams reflected from the mirror surface are possible, but since many astronomical measurements require extremely low background light levels we felt it advantageous to avoid shining any light on the mirror surface. In the light of these considerations we have invented a sensing system which monitors the segment positions without using the front surface. The segment positions and orientations are sensed by displacement sensors on the backs of the segments bridging the gaps between adjacent segments. These displacement sensors define all the degrees of freedom of the array except one, an overall "droop" or focus of the primary mirror. This last degree of freedom is defined by a tilt sensor measuring the relative tilt between two segments.

The array of actuators consists of three motor-driven roller screws on the back of each segment in order to control piston and two directions of tilt. A computer drives the actuators in response to the information from the sensors.

The analysis we describe here is a "quasi-static" one in the sense that we assume the perturbations of the surface take place on a time scale long compared to the sensor-actuator response cycle time (about 0.1 to 1.0 sec). This will be true for thermally induced distortions and gravitational loading changes. Whether or not the wind induced perturbations will be on a time scale smaller than or comparable to the cycle time is still unknown. We have initiated a program of measuring the wind forces on large existing telescope structures and optics. These measurements are being made under a variety of wind conditions and dome orientations and will provide the wind spectra needed to define the cycle time. Then an analysis of the dynamic response of the system will be made.

In Section 2 we describe in detail the geometry of the segments and the sensor and actuator characteristics assumed for this study. The algorithm for using the sensor information to control the orientation of the segments is described in Section 3. Using this algorithm in a computer simulation of the system we then establish the relationship between sensor precision and the image quality in Section 4. The image quality is first studied with geometrical optics and then diffraction theory is used to describe the image as a function of wavelength. The effects of systematic errors in the sensors are described in Section 5. The effect of noise in the actuators on the image is discussed in Section 6. Section 7 describes the results of studies of the system's sensitivity to component failures. Section 8 briefly discusses the practical implementation of a real time control system with existing computers. Finally, in Section 9 we summarize our results and discuss the general applicability of this method to larger arrays. Our analysis shows that the design is both feasible to construct and reliable. It is feasible to construct in the sense that sensors and mirror displacement actuators based on existing technology are capable of producing images of good optical quality using the above algorithm. Prototypes of sensors and actuators have been built and operate with better than the required precision. It is reliable in the sense that there is sufficient redundancy that the continuous figure control

operates even if some components fail. In addition, the recovery from an electrical power failure can be rapidly made. As presently designed, the displacement sensors are insensitive to power failure. Although the tilt sensor may lose its zero during a power failure, it can rapidly be recovered by refocusing the telescope.

2. Mirror and Control System Design

In concept the primary mirror will be an assembly of small infinitely stiff segments. The control system senses the location and orientation of the segments and moves them to maintain the desired surface. We briefly outline here our goals for the system. Our general approach is to keep the front surface as free as possible of obstructions by placing the sensing and actuating control elements on the back of the segments. This preserves the large collecting area and avoids additional light sources and scattering surfaces. The goal is to produce images either limited by atmospheric seeing or by diffraction. For wavelengths beyond 10 microns we expect diffraction effects to dominate the image quality. The system needs to provide rapid and continuous control in the presence of variable loading due to wind, gravity, etc. In addition it should be insensitive to the effects of power failures and component failure. Since it must operate all the time it must perform reliably, be easily monitored, and be readily maintained. Each mirror segment has six degrees of freedom. We characterize these as focus, rotation about two axes in the segment plane or "tilt", rotation about the normal to the segment, and finally radial and azimuthal motion of the segment center in the surface of the primary mirror. We assume in this study that only the first three motions are in need of active control. The remaining three motions will be passively constrained by the rigidity of the support structure. The analysis of the thermal and gravitational deformations of the support structure (Nelson and Mast, 1980c) shows that motions in the passively controlled degrees of freedom do not degrade the image quality.

In choosing a particular segment geometry we have tried to minimize the number of surface shapes, the number and complexity of control elements, and the number of different types of components. These objectives have led to the hexagonal design shown in Figure 1. The mirror consists of three "rings" of hexagonal segments with a total of 36 segments. Each segment is a regular hexagon when viewed from infinity. The number of segments was chosen on the basis of several technical considerations involving their fabrication and support (Nelson, 1980d). A larger number of segments requires more actuators and sensors; a smaller number makes the segment fabrication more difficult. Each segment has 0.9 meter edges with the area of the assembly being equal to that of a 10 meter diameter circular mirror. This design requires only one shape for the segment mirror blanks. The array of hexagons has a natural "interlocking" geometry which greatly simplifies the requirements for the control system. For this study we have assumed the figure to be a paraboloid with focal ratio f/1.75. The exact conic constants for the primary and secondary are still to be determined.

This design employs segments with 6 different off-axis paraboloidal surfaces. A technique for fabricating these off-axis surfaces has been developed (Lubliner and Nelson, 1980). The technique was successfully tested by fabricating a small off-axis paraboloidal mirror (Nelson etal, 1980b), and a full-scale demonstration is now in progress at Kitt Peak National Observatory.

The orientation of each segment is controlled by three displacement actuators arranged in a triangle on the back of the segment (Figure 2). In practice, each of the three actuators is attached to the segment through a 12 support point assembly to approximate a uniform support. There are a total of 108 actuators of identical construction. Each actuator contains a precision roller screw driven by a torque motor. Shaft encoders allow control of the actuator length to provide precise length changes in response to the information from the sensors. Tests of the prototype actuator show it will provide rapid positive control with a noise level less than the design goal of 50 nm.

There are 168 displacement sensors overlapping the edges of the mirrors (Figure 3). Each sensor measures locally the differences in heights of the surfaces of the two adjacent mirrors. By design these sensors are insensitive to displacements in the plane of the mirror or by any rotation or tilt about the center of the sensor. The height displacements are determined using a simple ratiometric capacitance measurement, and initial tests of a prototype are described by Gabor (1979, 1980). Low thermal expansion glass blocks are used for the capacitor plates and a bridge circuit has been used to achieve noise and drift levels much less than 50 nm.

The hexagonal geometry has a natural interlocking character which allows the use of the simple displacement sensors. This interlocking character is illustrated in Figure 4 showing a vertex where three segments meet. If the back two segments (A and B) are correctly oriented with respect to each other, then the measurements from the four displacement sensors shown can be used to calculate the orientation of segment C which is indented between the two. In particular, tilt of the segment C is measured by using the segment's stiff lever arm to convert positional information to angular information. This keystone effect operates between all the segments. In principle this single calculation could be used repeatedly from vertex to vertex to calculate the relative orientations of all segments in the array. In practice all of the sensor information is used simultaneously in a global fit, and this is described below in Section 3.

There are 108 degrees of freedom (3 per segment) which require active control. Three of these simply define the overall orientation of the primary mirror as a whole and these are defined by simply locking three of the actuators. Thus there are 105 degrees of freedom defining the relative orientations of the segments. The system of 168 displacement sensors measures (with considerable redundancy) all of these degrees of freedom except for one. The single last degree of freedom we call the "droop mode". This mode is most easily understood by imagining first an array of flat hexagonal segments lying in a plane so that the displacement sensors all read zero. Then, if all the segments are tilted and lowered (or raised) so that all their centers touch a common mathematical spherical surface, a droop mode distortion is induced. With this spherically symmetric distortion every set of three segments meeting at a vertex forms a triangular pyramid with each of the three segment normals tilted away from the vertex by the same angle. The geometry of this droop mode is such that every segment forms the same dihedral angle with respect to all its adjacent segments. In this distortion adjacent segments are simply "hinged" with respect to each other, leaving all the edges aligned and all displacement sensors reading zero. Since all the displacement sensors still read zero, this spherically symmetric distortion of the primary mirror is not measured by the array of displacement sensors. The effect on the optical image of this spherical distortion of the entire assembly is simply a change of focus, at least for small distortions.

In order to measure and thus be able to correct for this last degree of freedom we introduce a tilt sensor which measures the angle between the normals of two segments. The sensor consists of a light beam source mounted on one segment and a reflecting flat or cube corner assembly mounted on the second. The tilt angle measured is the angle between the projection of the normals onto a plane which passes through the segment center and the undisturbed normals. In practice we include three sensors for redundancy. These are shown to connect the segments at three corners of the array in Figure 3. It is also possible to use up to six tilt sensors and mount them on the edges of the outer corner segments of the array. This avoids the need for light beams crossing the primary mirror. As we will show below, a precision of about 0.1 arc second is required for the tilt sensor. Commercial instruments are available for making this measurement and we are in the process of evaluating their performance for this application.

Since there are many more sensors than actuators the system is highly redundant. Approximately two extra sensors per mirror provide both increased precision and stability. The redundant sensors also allow cross checks of sensor performance during the operation of the telescope. In addition they provide the extra information needed so that individual sensor failures do not disable the system.

3. Control Program

The control program uses the sensor readings to determine the desired actuator motion and thus adjust the mirror orientations in response to perturbations from the wind, from temperature changes, and from changes in the gravity loading of the support structure with steering. We emphasize again that the control system does not provide the initial alignment of the segments. A technique for making the initial alignment and the optical elements required for it will be described in a future publication. In addition a technique for periodic calibration of the sensors using stellar images will be described. In the present analysis we assume the alignment has been achieved and the control system described here is used to maintain that alignment.

For purposes of this study and without loss of generality we assume that when the mirrors are correctly oriented all of the sensors read zero. (In practice one will analyze the difference between the measured value and the desired one.) Perturbations then change the orientation of the segments and generate non-zero sensor readings. In the geometrical optics limit (zero wavelength) each segment of the paraboloid will make its own spot stellar image and the final image will contain 36 individual spots. Without perturbations or errors these will all superpose to form a single stellar image. With perturbations and errors a distribution of spots will be formed and the rms radius of this distribution is one measure of the image quality and control system performance.

The segment-sensor system is a complex coupled array and all sensors contribute some information about the orientation of each segment. Thus the calculation of the desired motion of the actuators relies on solving a set of coupled linear equations using all of the sensor measurements.

We have used a chisquare minimization technique to optimally use all of the information. In a system with no noise the expected reading on each sensor (tilt or displacement) is linearly related to the lengths of only the actuators on the two mirrors that it bridges.

$$s_j^{exp} = \sum_n A_{jn} p_n \tag{1}$$

where s_j^{exp} is the expected reading of the jth sensor and p_n is the nth actuator length. The matrix A_{jn} is defined by the geometry, and for the 36 segment system of Figures 1 - 3 the matrix has 171 x 105 elements. However, since each sensor measurement (including the tilt sensors) depends only on the lengths of the six actuators on the two defining mirrors, all but 6 elements of every row of the matrix are zero.

The chisquare is then defined

$$X^2 = \sum_j \frac{(\sum_n A_{jn} p_n - s_j^{meas})^2}{(\sigma_j)^2} \tag{2}$$

where s_j^{meas} are the actual measured sensor readings and σ_j their expected rms errors. The set p_n which minimizes chisquare is the solution to 105 coupled linear equations. The exact solution is found by effectively inverting A and has the form

$$p_k = \sum_n B_{kn} s_n^{meas}, \tag{3}$$

where the matrix B is completely defined by the geometry and the σ_j. The matrix B does not depend on the s_n^{meas} or p_n. In principle one finds the matrix B from A and σ_j just once for the system. Then to find the actuator motions needed to correct any perturbation (either real or due to noise) one takes the measured sensor values and performs the matrix multiplication indicated by equation 3. In the computer simulation of the control system described below we have used the very efficient algorithm of Golub and Reinsch (1970) to find the matrix B.

4. Displacement Sensor and Tilt Sensor Noise

Even without perturbations of the segments the sensors will have some intrinsic noise which will cause the control program to move the actuators and degrade the image from the ideal. Using the dimensions of the array and the assumed sensor noise levels we can first estimate the quality of the image by simple arguments. We then present the results of the full computer simulation of the control system.

Estimates Based on Geometry

The noise levels in the two types of sensors will be different. We assume the noise, σ_d, in all of the displacement sensors to be equal and the noise, σ_t, in all of the tilt sensors to be equal. Since the system is linear we expect the size of the blurred image coming from noise in a single type of sensor to be proportional to its rms sensor noise. The tilt sensor measures a degree of freedom of the assembly which is independent of those measured by the displacement sensors, thus we expect the effects of the two types of noise to be almost independent, and that the contributions to the image blur from each type of sensor can be added in quadrature. This will not be strictly true since a tilt sensor is coupled to the displacement sensors through the two particular segments it is mounted on. However, in practice, it is an excellent approximation.

We can estimate the size of the image blur from the displacement sensor noise alone using the dimensions in Figures 1-3 and an assumed sensor noise level of 50 nm. We expect the rms image size to be roughly given by 2(50nm)/(0.45m) = 0.05 arc seconds, where the factor of 2 and 0.45 m account for the ratio of the angular image motion to the angular mirror motion and the effective keystone lever arm. It is an important and remarkable fact that the strongly interlocked system allows the system error to be about the same as the single segment error estimated here. Thus, roughly speaking, errors do not propagate through the mirror.

We can also estimate the image blur size from tilt sensor noise alone using an assumed 0.1 arc second noise level in each sensor. In the droop mode the angle between two opposite outer segments equals the radius of the image. For the configuration of 3 tilt sensors (Figure 3) each sensor measures $\sqrt{3}/2$ of the angle between the outer segments; so the image radius is $2/\sqrt{3}$ of the reading. The rms radius including all segments is about $1/\sqrt{2}$ times this outer radius. For 3 sensors the noise is reduced by $1/\sqrt{3}$. So we can roughly expect an rms image radius of $(0.1)(2/\sqrt{3})(1/\sqrt{2})(1/\sqrt{3}) = 0.05$ arc seconds.

Combining the displacement and tilt rms image radii in quadrature gives an estimated rms image radius of 0.07 arc seconds for the assumed levels of sensor noise, $\sigma_d = 50$ nm and $\sigma_t = 0.1$ arc seconds.

For observations in the infrared, where near diffraction limited performance may be achieved, the correct phasing as well as the tilt of the segments is important. Noise in the sensors and actuators generate tilt and phasing errors and thus a primary mirror surface which differs from the ideal one. The difference between the ideal and achieved surfaces is an error surface. To characterize the surface roughness we define the "rms surface error" to be the rms deviation of the error surface about its mean.

As we did for the image blur we can make rough estimates of the size of the rms surface error using simple geometrical arguments. For a system with displacement sensor noise alone a very rough estimate of the surface error is obtained by assuming the middle ring of 12 segments defines the average surface, and the tilting of the 24 inner and outer ring segments move their centers away from the average. Based on the 0.05 arc second rms image radius estimated above, the rms mirror tilt angle will be 0.025 arc seconds. The distance of the inner and outer ring segments from the middle ring is about 1.5 m. The product of these weighted by the number of mirrors (24/36) gives a rough estimate for the rms surface error of 0.13 microns.

For a system with tilt sensor noise alone the rms surface error can be simply and accurately estimated using the formula for a paraboloid, $z = \rho^2/2k$, where k is the radius of

curvature. The error surface generated by tilt sensor noise, corresponding to a change in focus of the paraboloid, is equal to $dz = (\rho^2/2k^2)\delta k$. The rms deviation of this surface about its mean is readily calculated and related to the slope at its edge to show that a 0.1 arc second tilt sensor noise gives an rms surface error of 0.12 microns.

Combining the surface errors from tilt and displacement sensors in quadrature gives an estimated rms surface error of 0.18 microns for the assumed levels of sensor noise $\sigma_d = 50$ nm and $\sigma_t = 0.1$ arc seconds.

All segments are not alike in their contributions to the image error and it is interesting to look at the contributions of each type of segment to the image size. We define eight mirror types in Figure 5 according to their distance from the primary center. For a system with no tilt sensor error the global assembly should be in focus and the displacement sensor errors will cause tilt and piston of the segments within the ideal global shape. Thus, neglecting edge effects, we expect for $\sigma_t = 0$ that the image blur contribution will be independent of the mirror type. Alternatively for a system with no displacement sensor noise ($\sigma_d = 0$) the tilt sensor noise will cause a global flexing of the assembly so that the 36 individual images move radially in and out; corresponding to a change in focus. For this case the segments at larger radii will contribute more to the image blur.

Result of Computer Analysis

We have used the control system program to study the image blur quantitatively. The segments were assumed to be in their ideal orientation and random sensor noise was generated with a gaussian distribution of width σ_d for the displacement sensors and σ_t for the tilt sensors. The best fit for the actuator lengths to match the sensor values was calculated, the segments were moved using those actuator lengths, and the resulting image was analyzed. Figure 6 shows a typical spot diagram ($\sigma_d = 50$nm, $\sigma_t = 0$). The procedure was repeated with 100 sets of random sensor errors to obtain smooth distributions. The image distribution, a superposition of 100 spot diagrams, can be approximated by

$$P(\theta)\theta d\theta d\phi = \frac{1}{2\pi\delta^2}\exp(-\theta^2/2\delta^2)\theta d\theta d\phi \qquad (4)$$

The parameter δ, the one dimension gaussian width, is $(1/\sqrt{2})$ times the rms radius of the two dimensional distribution. For this distribution, the enclosed energy in a circle of radius r is given by $1 - \exp(-r^2/2\delta^2)$. The image radii which contain 80% and 90% of the energy are $r(80\%) = 1.8 \delta$ and $r(90\%) = 2.1 \delta$.

For the system described in Figures 1-3 with perfect noise-free tilt sensors ($\sigma_t = 0$) and with displacement sensor noise σ_d, we found the image parameter δ to be related to σ_d by $\delta = 0.72\sigma_d$, where δ is in arc seconds and σ_d is in microns. Alternatively, with the displacement sensors noise free and the tilt sensors with a noise level of σ_t we found the parameter δ to be given by $\delta = 0.38\sigma_t$, where δ and σ_t are in arc seconds. These two relations are the basic results of the study relating sensor noise to image quality.

Our expectation that the effects of the two types of sensor errors can be added in quadrature is confirmed by the computer study. The results are illustrated in Figure 7 where a fixed displacement sensor error of 50 nm was used and the tilt sensor error varied. The total error shown is everywhere within 5% of that expected by adding the two errors in quadrature.

Using this quadrature relation and the results in Figure 7, the image size r(80%) as function of σ_d and σ_t can be calculated and it is shown in Figure 8. A displacement sensor noise of 50 nm and a tilt sensor noise of 0.1 arc seconds gives r(80%) = 0.097 arc seconds which is consistent with the design goal for the Ten Meter Telescope, r(80%) = 0.16 arc seconds.

Primary mirrors composed of 2 and 4 rings were also investigated, and the parameter δ for $\sigma_d = 50$ nm and $\sigma_t = 0.1$ arc seconds is shown in Figure 9. For each configuration the tilt sensors were always on the outer ring. Again the quadrature adding of the two contributions is

valid. The important and encouraging feature is the stability of δ as the number of rings increases. We conclude that with the assumed sensor noise levels it is possible to build very large primary mirrors and still have the image quality effectively undegraded by the sensor errors. A segmented primary mirror with 4 rings of segments, each 1.05 meters on an edge, has a collecting area equal to that of a 15 meter diameter circular mirror. For such a mirror the image blur due to sensor noise will be no worse than that for the 10 meter mirror described here.

The images formed by the segments of each type were also analyzed, and the results confirm our qualitative expectations described above. The behavior of δ as a function of mirror type for primaries with 2, 3, and 4 rings is shown in Figure 10. For a system with no tilt sensor noise the image blur contributions are almost independent of mirror type. For a system with no displacement sensor noise the image blur contributions are just those expected from the geometry of the droop mode. The two contributions add in quadrature to accurately approximate the results with both types of noise shown in Figure 10 (σ_d = 50nm and σ_t = 0.1 arc seconds).

The rms surface error defined above is a second characteristic of the control system performance. We have calculated the surface error for the cases of displacement sensor noise alone, tilt sensor noise alone, and two combined for 2, 3, and 4 ring arrays. The results are shown in Figure 11. For the three ring system the rms surface error is related to the sensor noises by the following relations: $dS(\mu m) = 3.08\sigma_d(\mu m)$ and $dS(\mu m) = 1.04\sigma_t$(arc seconds). With noise levels of σ_d=50 nm and σ_t=0.1 arc seconds, the rms surface errors due to each type of sensor noise are 0.154 μm and 0.104 μm respectively. These agree with our rough estimates based on geometry. The computer simulations also show that these surface errors come almost entirely from the pistoning of the segment centers, and not from the tilt of the segments about their centers. The rms surface error coming from both types of sensor noise together is also shown in Figure 11. To an accuracy of about 10% the two individual noise contributions can be added in quadrature to approximate the effect of both.

The dependence of the rms surface error on the number of rings is different than that of the rms image size. It is thus a somewhat independent measure of the control system performance. Unlike the image radius, the rms surface error increases with the number of rings. For the 3 ring system and assumed sensor noises of 50 nm and 0.1 arc seconds the resulting rms surface error is 0.21 μm. At a wavelength of 10 μm this is about $\lambda/50$ and thus will not significantly degrade the diffraction limited performance. For a system with 4 rings the rms surface error is 0.26 μm and the sensor noises would need to be somewhat smaller than those assumed here to not degrade the diffraction limited performance.

All of the above analysis used geometrical optics assuming the wavelength of light to be negligible. To understand the effects of discrete steps in the surface the analysis was repeated using the diffraction theory of aberrations (Born and Wolf, 1980). The best fit actuator solution for each set of random sensor noise gives a specific surface for the primary. This surface was used in a Kirchoff-Fresnel integral to calculate the image plane energy distribution taking into account the interfering contributions from each differential area of the mirrors. The final image distribution was characterized by the radius containing 80% of the energy. The calculation was based on the procedure described in Born and Wolf and used the expression for the diffraction pattern of a hexagonal aperture (see Mast etal, 1982). The coma for the assumed f/1.75 paraboloidal mirror was included and it increased the calculated image sizes by about 8%. Assuming again σ_d = 50nm and σ_t = 0.1 arc seconds, the parameter r(80%) was calculated, and it is plotted as a function of wavelength in Figure 12.

For small wavelengths the 80% radius matches that expected from geometric optics. As the wavelength increases, each spot of the spot diagram becomes a diffraction pattern for an individual segment, and r(80%) increases. As the wavelength becomes much larger than the rms surface error, the image approaches the diffraction pattern of the whole primary. An additional analysis of diffractive effects, including the effects of the cracks between the segments, is described by Mast etal (1982).

5. Systematic Sensor Errors

In the preceding section we described the effects of statistical sensor noise. A set of real sensors will also display a variety of systematic errors. These errors will be caused either directly or indirectly by thermal, gravitational, or aging effects. Indirect effects would result from initial fabrication or mounting errors in the sensors. For example, a misalignment of the sensor components will make the sensors sensitive to thermally induced segment motion in the passively controlled degrees of freedom.

Before discussing the effects of these errors we note that the control algorithm itself provides a continuous indicator of the presence of these errors. Systematic errors will in general make their presence known in the value of the chisquare that is calculated at each control step. Systematic changes in a single or few sensors will be immediately detected by an increase in the particular terms in the chisquare sum associated with those sensors. Systematic changes in all the sensors will increase the overall chisquare.

Although most systematic shifts will affect the chisquare, it is mathematically possible to find sets of systematic shifts in the sensors which do not change the chisquare at all and yet still degrade the image. For example, such a set is generated by tilting the segments away from their ideal positions and then resetting the ideal sensor readings to be those generated by the tilting. Such sets of systematic shifts are only expected to occur from errors in the initial alignment procedure or software errors. They have a vanishingly small probability of being generated from thermal, gravitational, or aging effects, since they represent a 105 dimensional subspace of the full 171 dimensional sensor space.

More plausible sets of systematic errors will be generated by gravitational, thermal, and aging effects. We expect the size of these errors to vary smoothly and slowly with the sensor position in the primary mirror. Thus we have studied the effect on the image of various low spatial frequency distributions of displacement sensor shifts.

The effect of low spatial frequency shifts in the sensors is smaller than that of statistical noise due to the high level of redundancy and symmetry in the control geometry. The design of each displacement sensor makes it asymmetric; one side containing a "body" and the other a paddle which bridges the gap between two segments and fits into the body. Figure 13 shows schematically the orientation of these sensors on a segment. If all sensors experience an equal systematic drift from their correct value (of 0), then chisquare will increase, but at each vertex the two nearby sensors will "pull" the segment corner in opposite directions. Thus there is a canceling effect which reduces the image degradation caused by the shifts. An alternative way to understand this is to realize that the three sensors surrounding a vertex have the characteristic that the sum of their three signals should nearly vanish. This is true independent of any mirror motions to the extent that the three sensors are all close to the same point, the vertex. If the readings of these three sensors give a non-zero sum, then the effect of the least squares algorithm will be to subtract a third of the sum from each sensor in calculating the segment positions. Thus, again, if there are equal errors in the three sensors, no erroneous segment motion will occur. (We emphasize that we only mention this approximate zeroing of the sum of the three sensors at a vertex to give an additional intuitive understanding for the system. This constraint is of course already built into the control algorithm equations and doesn't require any additional equations or analysis.) These canceling effects occur at those vertices where there are three sensors. However, there is an inner ring and outer ring of vertices which have only one sensor (see Figure 3); thus the system as a whole does have some sensitivity to constant systematic shifts.

The lowest spatial frequency distribution of errors will be a constant or uniform distribution, i.e. the same shift in the readings of all displacement sensors. Examples of these identical systematic errors include thermally induced offsets in the sensor electronics, gravitationally induced deformations of the sensor components, and gravitational deformations of the segment edges where the sensors are mounted. Even drift from aging sensors, sensor fabrication errors, and mounting misalignments may have a large constant component in their distribution. To find the effect of the systematic shift alone we have set the sensor noise to zero and added a 50

nm shift to all the displacement sensors in the control program. The resulting fit gives a chisquare of 159 compared to 66 for noise alone. The resulting image size is a factor of 8.7 times smaller than that due to sensor noise (σ_d=50nm, σ_t=0.1 arc seconds). The rms surface from the fit is 24 times smaller than that due to sensor noise. Thus a uniform shift in the sensor readings will readily be detected in the chisquare, and the shift will need to be 8.7 times as large as the sensor noise to have the same effect on the image.

We have also calculated the effect on the image of other distributions of systematic errors. For distributions of the form X, Y, $2X^2 + 2Y^2 - 1$, $X^2 - Y^2$, and 2XY the image sizes are smaller than that due to noise by the factors 2.5, 2.5, 4.8, 1.9, 1.9, respectively. The rms surface errors are smaller by similar factors, and again there is a substantial increase in chisquare.

Systematic errors in the three tilt sensors have also been investigated. A systematic change in the tilt sensor readings can be separated into two types or components; one where there is a shift in the average value of the three readings and one where there is a non-zero rms dispersion around a zero average. For example, the two sets of shifts, (0, +1, -1) and (-1/$\sqrt{3}$, -1/$\sqrt{3}$, 2/$\sqrt{3}$) both have zero average shift, and both have the same rms dispersion of $\sqrt{2/3}$. They do have a different skewness, but empirically only the first two parameters are significant.

For a set of systematic shifts with a non-zero average, there will be a direct change in the focus of the overall assembly. The resulting degradation of the image is just given by the scaling described above in section 3; r(80%) = 0.38 s, where s is now the shift in the average of the three tilt sensor shifts in arc seconds. In principle this error is removable by refocusing the telescope. If there are also systematic errors which cause a non-zero dispersion of the three tilts, this corresponds to a non-focus distortion. This distortion couples to all of the degrees of freedom measured by the displacement sensors. Since there are so many displacement sensors they tightly constrain the system and reduce dramatically the effects of the tilt sensor dispersion on the image. For the system described in Figures 1-3 we have investigated the effect of the two sets of systematic shifts (-1, 0.0, 1) and (-1/$\sqrt{3}$, -1/$\sqrt{3}$, +2/$\sqrt{3}$). We find the image size from the tilt and displacement noise combines in quadrature with a "reduced" tilt sensor dispersion. The tilt sensor dispersion is reduced roughly by the expected factor $\sqrt{168/3}$. This large reduction makes the system relatively insensitive to tilt sensor dispersion. The effect of the skewness is small.

We conclude from these studies of systematics that the redundancy and symmetry of the control geometry make the control system substantially less sensitive to systematic errors than to statistical errors.

6. Actuator Noise

Following a procedure similar to that used for the sensor noise we have calculated the effect of actuator noise on the image. By "noise" we mean the inability of the actuator to move the commanded distance to better than the indicated noise figure. The noise in a sensor effects more than one segment and thus contributes in a coupled way to the final image quality. Noise in an actuator effects only one segment, and thus the effect on the image quality is more simply calculated. The image parameter δ is proportional to the rms actuator position error, and for the assumed design (Figure 2) we find δ(arc seconds) = 0.53 δp(microns). The rms surface error is given by the expression dS(microns) = 0.94δp(microns). For actuator errors of 50 nm, δ is 0.026 arc seconds and the rms surface error is 0.047 microns. The contributions from sensor noise and actuator noise can be added in quadrature. For the design in Figures 1 - 3, with σ_d=50 nm, σ_t=0.1 arc seconds, and σ_a=50 nm, the combined parameter δ is 0.060 corresponding to r(80%)=0.108 arc seconds.

7. Component Failures

Using geometrical optics we have investigated the effects of sensor failures. Since the sensor designs being considered are simple in construction and expected to be reliable, the number of sensor failures in practice is expected to be quite small.

We have calculated the image degradation when randomly chosen sets of sensors are eliminated from the system. After choosing the sensors to delete, one recalculates the B matrix and performs the same analysis previously described. The degradation of the image increases slowly with the number of sensors eliminated, and for a system with 20 sensors eliminated the rms image size is increased by only 20%. We conclude that the multiple ways the segments are related through the sensor array and the large sensor redundancy combine to form a very stable system of control.

In practice, defective sensors can be identified by monitoring each sensor's contribution to chisquare. If a sensor's average contribution begins to substantially exceed its expected value, it can be labeled defective. The A matrix can be reconfigured without the suspect sensor and the B matrix recalculated. This reconfiguration will take a longer time than the control cycle time. During this reconfiguration the sensor reading can be fixed at its average normal value.

An alternative to reconfiguring the matrix may be to simply leave the sensor reading fixed at its average normal value. The redundancy of the system means that the error introduced will have only a small effect on the overall performance. However, there may occur large perturbations for which the average value is seriously in error. We have investigated this alternative approach to sensor failure and its response to large perturbations. We find that the system requires several sensor-actuator cycles to recover from a large perturbation when a sensor is fixed to read its average value. Each cycle however produces a factor of about 3 improvement in the fit so the number of cycles required to reconfigure the mirror is not large. Because of this it appears that a practical alternative for handling defective sensors (until they can be repaired or replaced) is to simply replace the actual sensor reading by its nominal one. The virtue of this technique is that the relatively time consuming process of generating a new B matrix can be avoided. As discussed below it is expected the B matrix generation will require about 150 times as long as a normal correction cycle.

Because of the lack of redundancy, the actuator failures are more critical than sensor failures. There are three actuators, however, that need to be fixed or frozen in order to define the orientation of the overall primary mirror with respect to the mirror support structure. Any three actuators can be used to provide this definition. If an actuator fails, it can then simply be used as one of the three fixed, defining actuators. Thus up to three actuator failures can occur without degradation of the system.

8. Real Time Control

The computations for the control system are of two types described above. The longer process is the "inversion" for solving the coupled set of linear equations. This needs to be performed only occasionally when, for example, a sensor fails. The number of mathematical operations for this inversion scales as the number of sensors times the number of actuators squared, $(171)(105)^2$. The calculations for this paper were performed on a CDC 7600 computer which uses 140 ns of central processor time per multiplication. Modern small computers are also becoming available with comparable multiply times. The inversion required a total of 2.4 seconds and 60,000 words of memory.

Given the inversion, the actuator movements needed to respond to a set of sensor readings are calculated with a single matrix multiplication. For the CDC 7600 this required 15 milliseconds. This time is sufficiently small to allow the control system to correct perturbations with frequencies less than about 10 Hz. Recent improvements in the speed of small computers, and the availability of vector processing machines, should allow the control system cycle time to be made almost arbitrarily small.

9. Summary

As the size of the telescope primary mirror is increased the mass of the mirror needed to maintain a given image quality increases enormously (as approximately the third power of the diameter). To avoid this tremendous scaling of the mass (and cost) of the mirror and its support structure mirror designs consisting of an assembly of many small segments have been proposed. The central challenge of these designs is the creation of an economical and reliable system to sense and control the orientations of the segments. A specific design employing hexagonally packed segments has been proposed for a new 10-meter telescope for the University of California. The interlocking character of the hexagonal geometry allows measurement of the mirror segment orientations with simple capacitive displacement sensors and a single angle measuring tilt sensor. Information from these sensors is then used to control the orientations of the segments and maintain the figure of the primary in response to perturbations of wind, gravity loading, and temperature changes.

We have made a computer analysis of such a control system. The program that would be used to actuate movement of the segments in response to the sensor information has been written. Using this program we have quantitatively established the effects of sensor and actuator noise on the image quality. The image size scales linearly with the rms errors in the sensors and actuators. For assumed values of displacement noises of 50nm and tilt sensor noises of 0.1 arc seconds the image gaussian widths are 0.036 and 0.038 arc seconds respectively. seconds. For an actuator noise of 50 nm the resulting image gaussian widths is 0.026 arc seconds. Combined in quadrature these give a width of 0.060 arc seconds and thus 80% of the energy is contained in a circle of 0.11 arc second radius. Based on initial estimates and tests of the sensors and actuators the assumed errors should be easily achieved. The resulting image size is well within the design goals of the 10-meter telescope and of course less than the atmospheric seeing for visible light. A diffraction analysis for the same assumed error levels shows the image will not be degraded from diffraction limited performance at 10 microns by sensor or actuator noise.

The program was also used to test the sensitivity of the system to sensor failures and showed the image size degrades only very slowly as sensors are eliminated. This confirms our expectation that the sensor redundancy makes the control very stable.

In addition to investigating the image quality for the 10-meter telescope we have also studied the image quality as more segments are added. The size of the image does not change with more rings of segments, and we conclude that the images from primary mirrors of even larger assemblies would not be degraded by sensor and actuator noise.

References

Born, M. and Wolf, E., *Principles of Optics*, 6th Edition, Pergamon Press (1980)

Crane, R., *Optical Telescope Technology Workshop, Nasa Report SP-233* (April 1969) p. 297 "Figure Sensing Techniques."

Gabor, George,. *Proceedings of the Society of Photo-Optical Instrumentation Engineers*, 172 (January 1979a), "Position Sensors and Actuators for Figure Control of a Segmented Mirror Telescope."

Gabor, G., *Proceedings of Kitt Peak National Observatory Conference on Optical and Infrared Telescopes for the 1990's* (Tucson, Arizona, January 1980) p. 587, "Displacement Sensors and Actuators Needed to Control a Segmented Primary Mirror."

Golub, G.H. and Reinsch, C., *Numerische Mathematik,* 14 , 403-420 (1970)

Hardy, J. W. *Optical Telescopes of the Future, Conference Proceedings*, p. 455 (December 1977), Geneva 23: ESO c/o CERN 1978. "The Role of Active Optics in Large Telescopes"

Lubliner, J. and Nelson, J.E., *Applied Optics*, 19 , 2332 (July 1980), "Stressed Mirror Polishing. 1. A Technique for Producing Non - Axisymmetric Mirrors."

Mast, T. and Nelson, J. *Proceedings of Kitt Peak National Observatory Conference on Optical and Infrared Telescopes for the 1990's* (Tucson, Arizona, January 1980) p. 508, "Figure Control for a Segmented Telescope Mirror."

Mast,T., Nelson, J. and Welch, W.J., *Ten Meter Telescope Report #68 (January 1982)* "The Effects of Primary Mirror Segmentation on Image Quality."

Nelson,. J., *Optical Telescopes of the Future, Conference Proceedings*, (December 1977), p. 133, Geneva 23: ESO c/o CERN 1978 "The Proposed University of California 10 Meter Telescope."

Nelson, J., *Society of Photo-Optical Instrumentation Engineers Proceedings*, 172 (January 1979), "Segmented Mirror Design for a Ten-Meter Telescope."

Nelson,J., *Proceedings of Kitt Peak National Observatory Conference on Optical and Infrared Telescopes for the 1990's* (Tucson, Arizona, January 1980a) , p. 11, "The University of California Ten Meter Telescope Project - The Segmented Design."

Nelson, J.E., Gabor, G., Hunt, L.K., Lubliner, J., and Mast, T.S., *Applied Optics,* 19, 2341 (July 1980b), "Stressed Mirror Polishing: 2. Fabrication of an Off-axis Section of a Paraboloid."

Nelson, J.E. and Mast, T.S. *Ten Meter Telescope Report # 48* (October 1980c), "Mirror Segment Motions from Gravitational Deformation of the Cell."

Nelson, J.E., *Ten Meter Telescope Report # 41* (1980d), "The Size and Number of Primary Mirror Segments."

Figure Captions

(1) The geometry of the segmented primary mirror with three rings of hexagonal segments and a total of 36 segments. The area is equal to that of a ten-meter diameter circular mirror.

(2) The location of some of the 108 actuators shown schematically on the backs of the mirror segments. The actuators control the orientation of the segments by moving normal to the segments.

(3) The positions of the 168 displacement sensors and three tilt sensors used for sensing the relative orientations of the mirror segments.

(4) Schematic plan and oblique views of three mirror segments illustrating the displacement measurements made by the sensors.

(5) Definition of the mirror segment types labeled according to their distance from the center of the primary.

(6) A typical image spot diagram generated by 50nm of displacement sensor noise and 0.0 arc seconds of tilt sensor noise.

(7) The one-dimensional gaussian width δ (arc seconds) of the image spot distribution for a 50nm noise level in the displacement sensors as a function of tilt sensor noise. The straight line is the width for a system with no displacement sensor noise.

(8) A contour plot of equal level of radius (arc seconds) enclosing 80% of the energy as a function of the noise in the tilt sensor (arc seconds) and the noise in the displacement sensors (nm).

(9) The image width parameter δ (arc seconds) for systems with 2, 3, and 4 rings of segments. The lower points are for systems with (a) tilt sensor noise alone (0.1 arc seconds) and (b) displacement sensor noise alone (50nm). The upper points (c) are for both types of noise together.

(10) The gaussian width parameter δ in arc seconds as a function of mirror type for primary mirrors of 2, 3, and 4 rings of segments. We assume $\sigma_d = 50$ nm and $\sigma_t = 0.1$ arc seconds.

(11) The rms surface error (μm) for systems with 2, 3, and 4 rings of segments. The lower points are for systems with (a) tilt sensor noise alone (0.1 arc seconds) and (b) displacement sensor noise alone (50 nm). The upper points (c) are for both types of noise together.

(12) The radius (arc seconds) enclosing 80% of the energy as a function of wavelength, determined from a diffraction calculation. A displacement sensor noise of 50nm and a tilt sensor noise of 0.1 arc seconds have been assumed. The straight diagonal line is the image size expected from a perfect mirror.
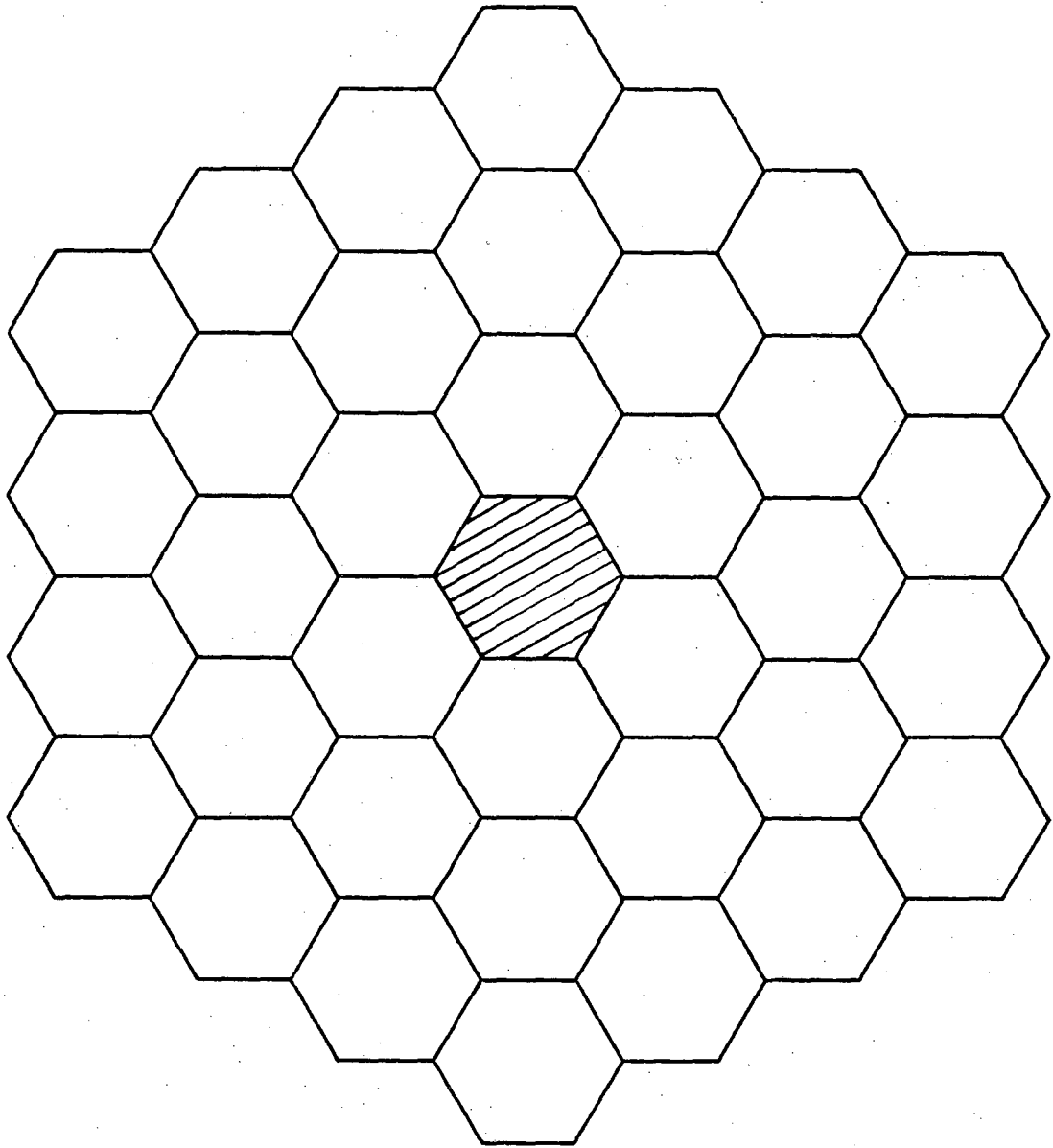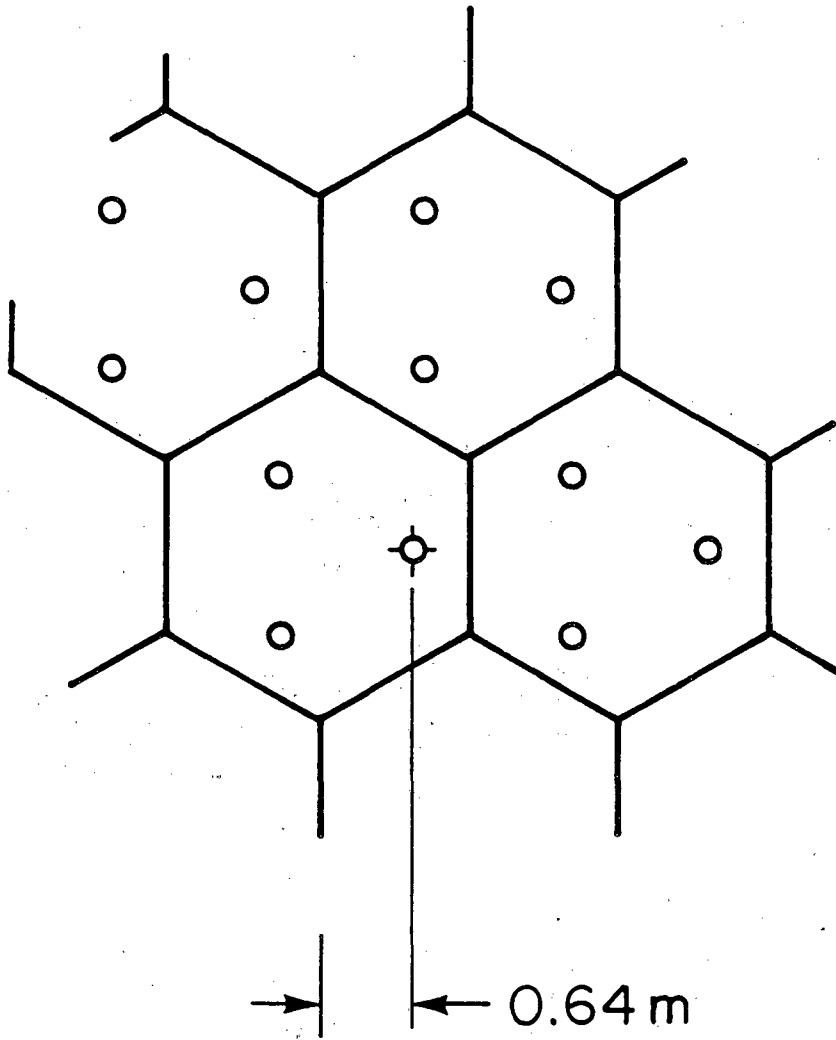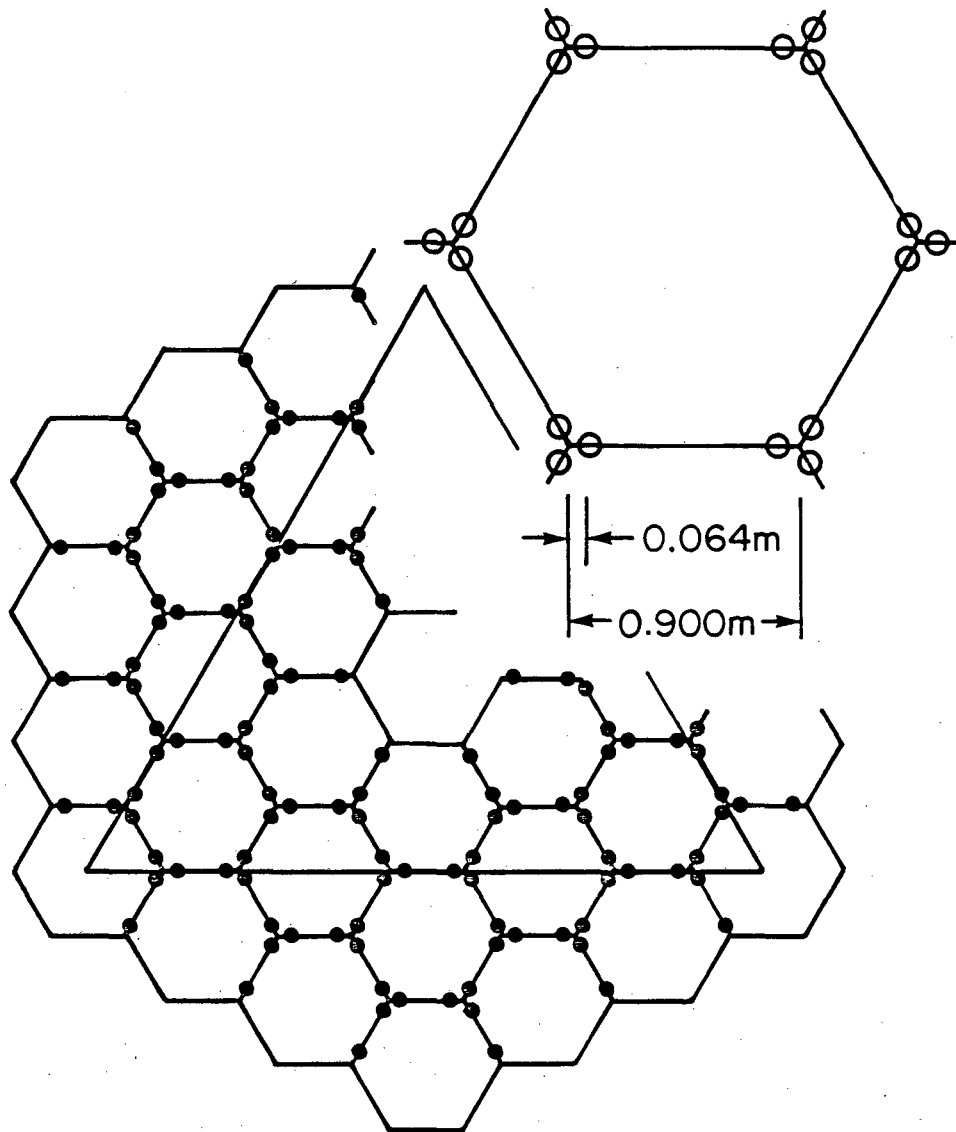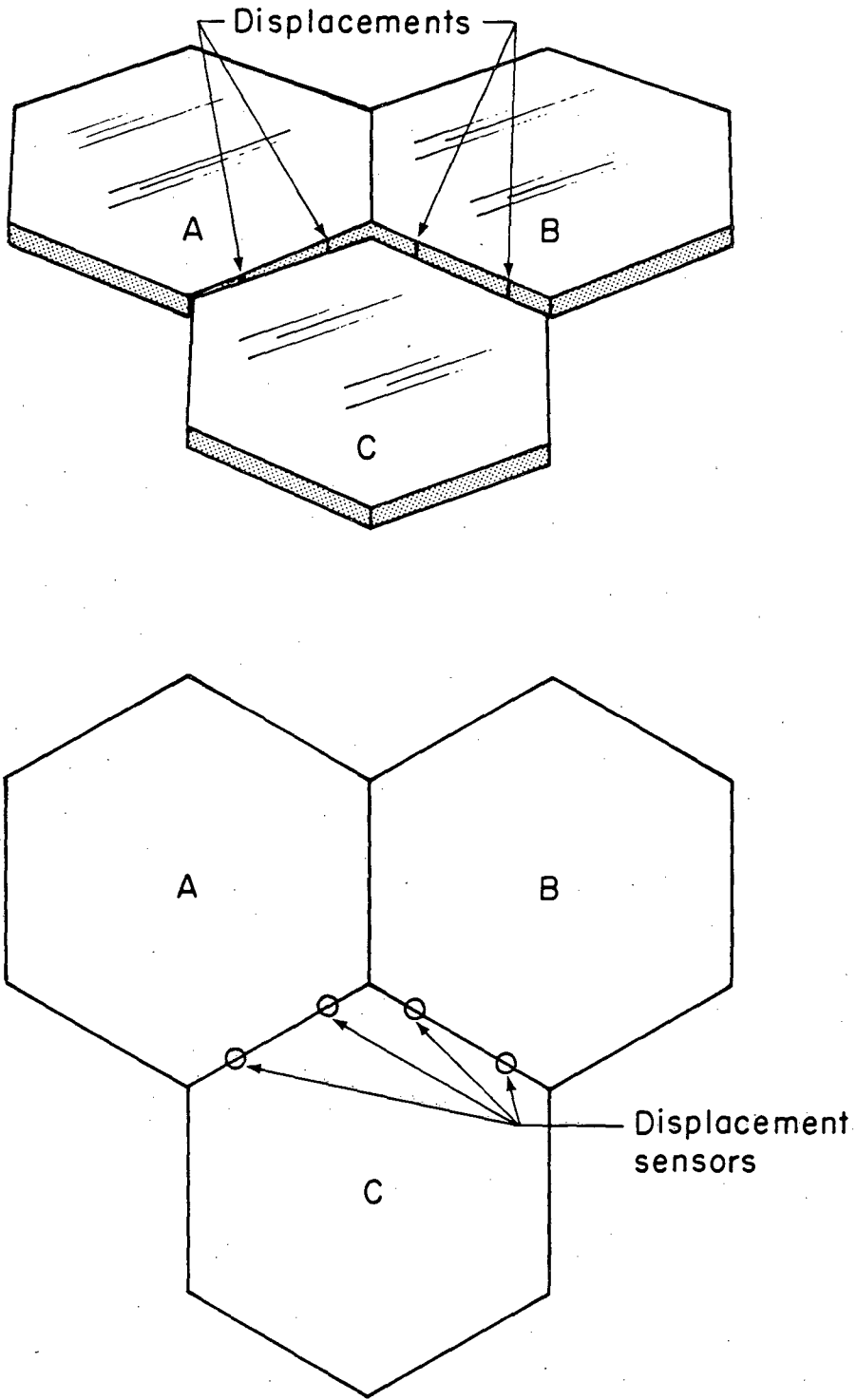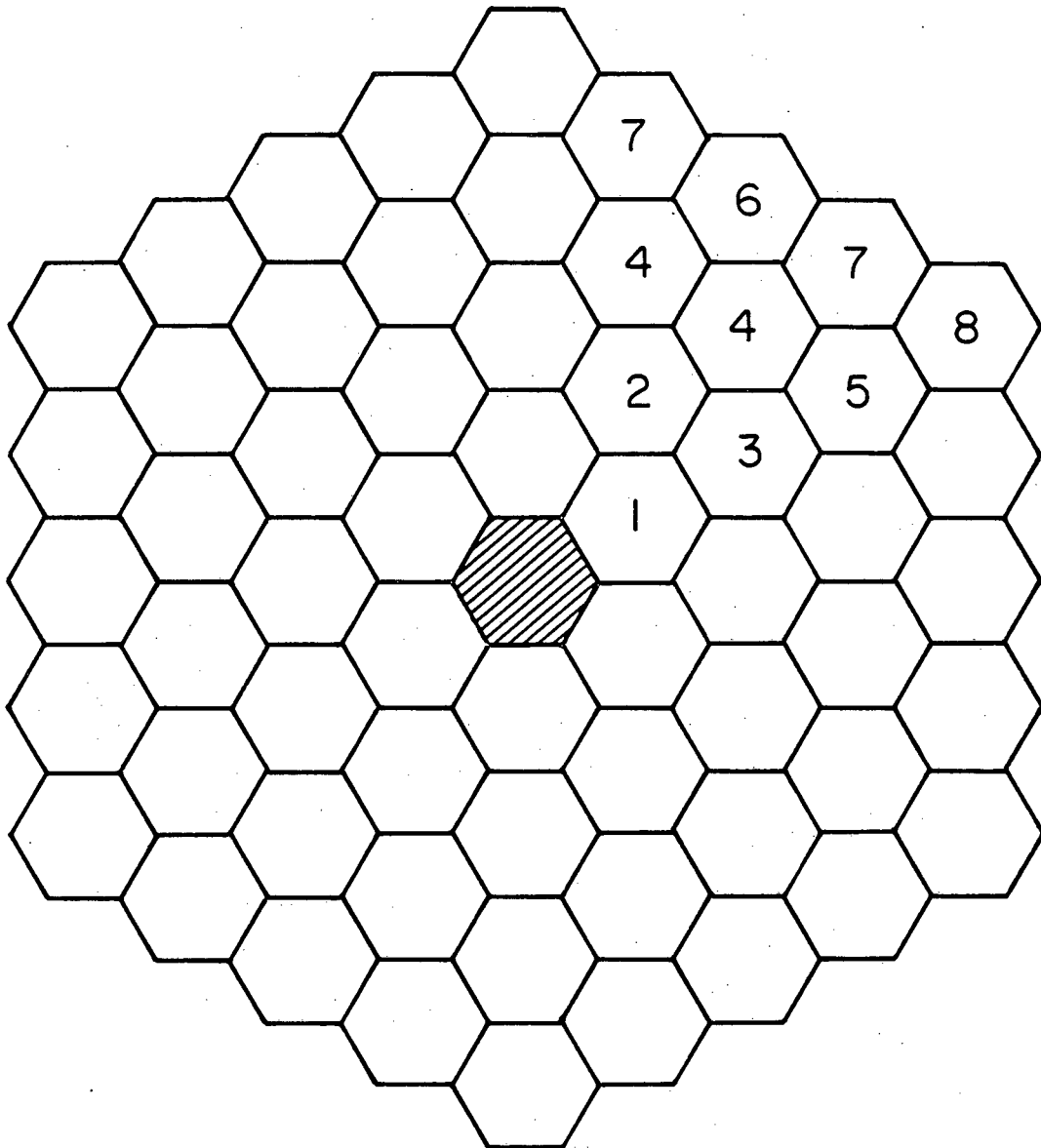
| .9m |

10.0m
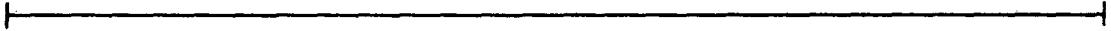
XBL 8012-13621

Figure 1

XBL 817-2397

Figure 2

0.064m

0.900m

XBL817-2396

Figure 3

Figure 4

XBL 817 – 2405

XBL 817 – 2395

Figure 5
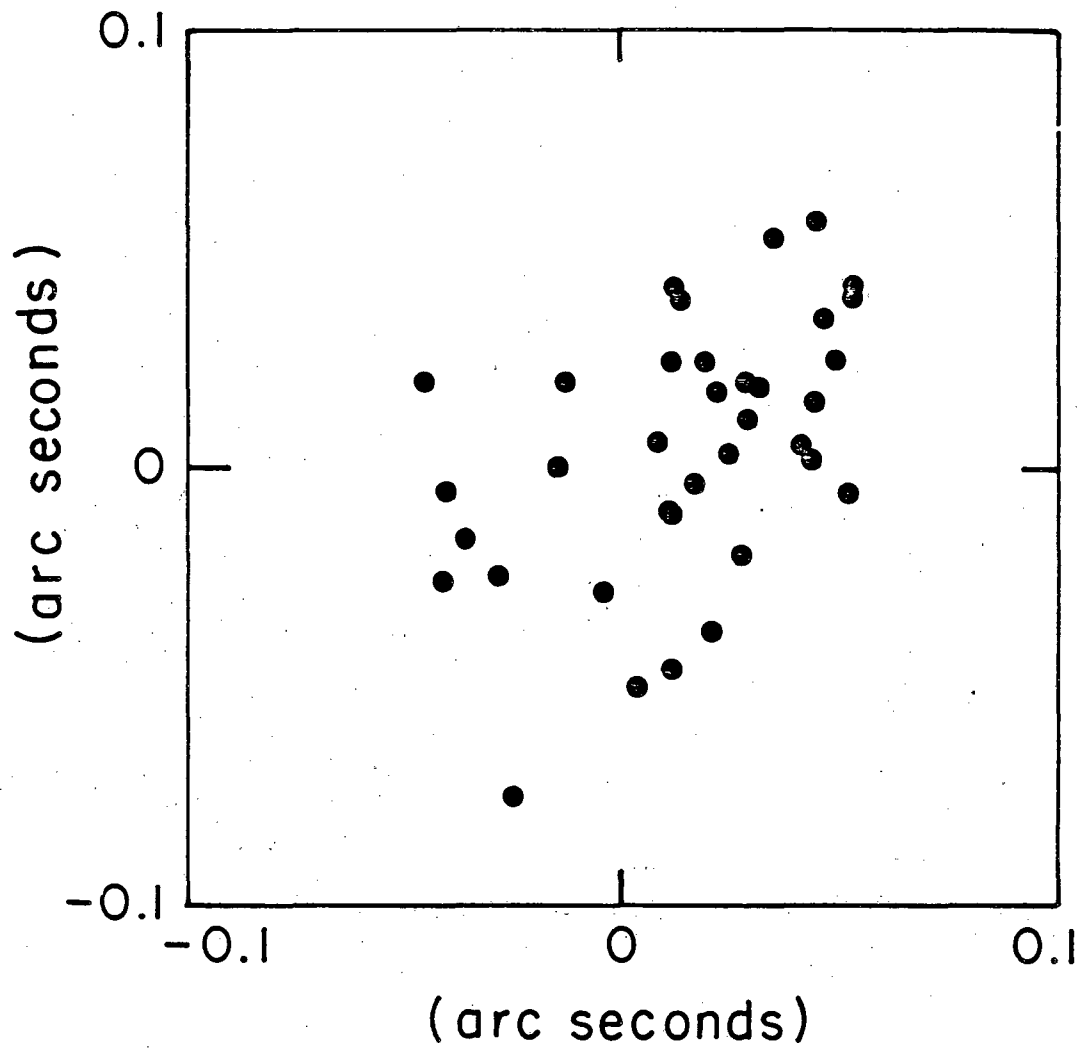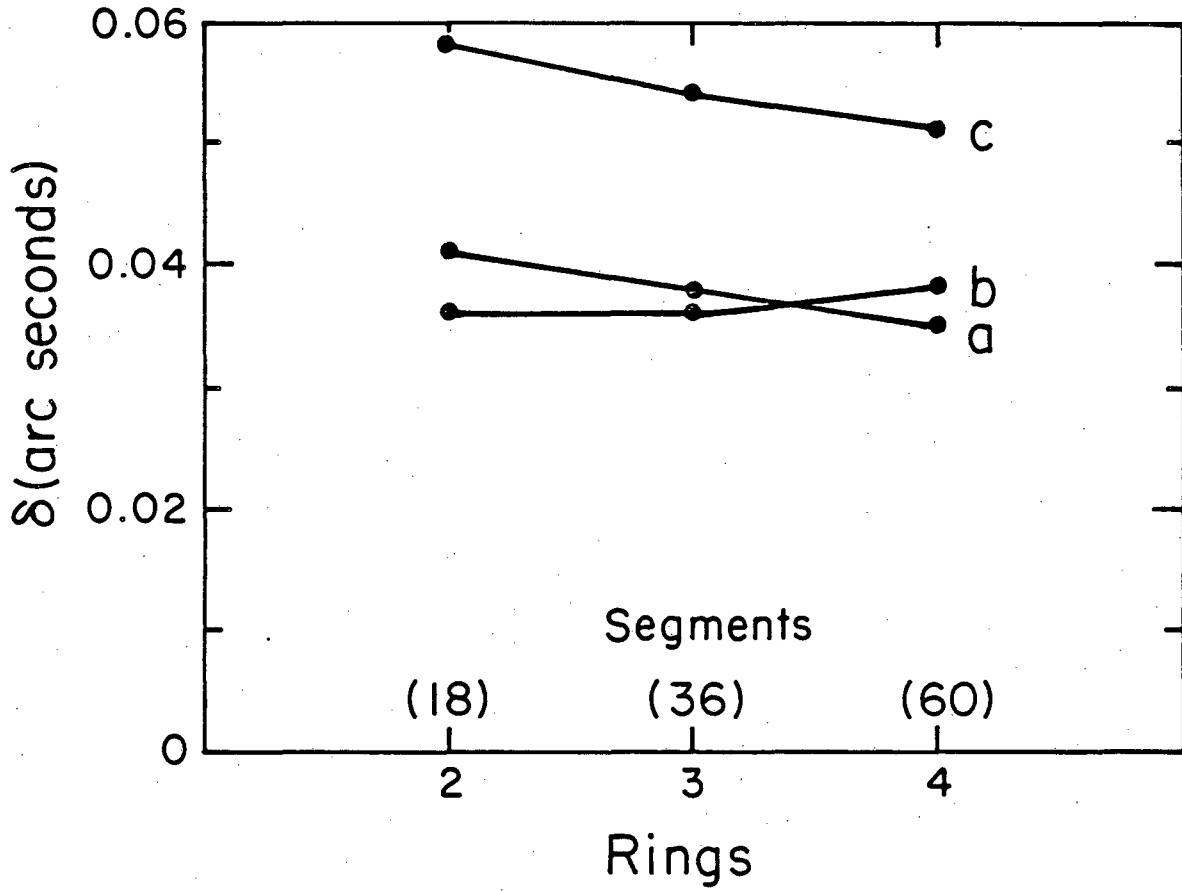
XBL817-2403

Figure 6
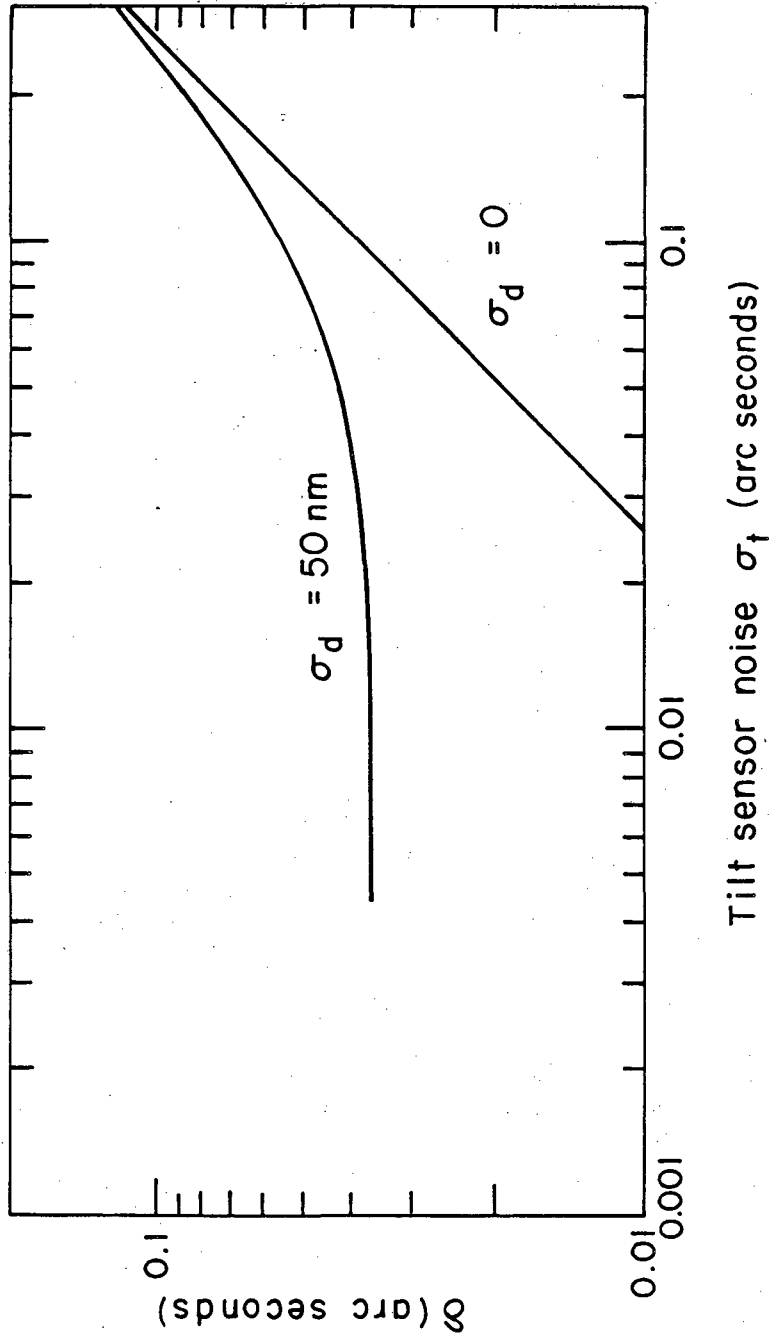
Figure 7

XBL 817–2402

Figure 8

XBL817-2401

XBL 817 — 2398

Figure 9

Figure 10

XBL817-2400

Figure 11

Figure 12

XBL 817−2404

Wavelength (μm)

r (80%) (arc seconds)

Geometric optics limit

XBL 821-4400

Figure 13